PCCP

Two-dimensional infrared spectroscopy from the gas to liquid phase: Density dependent *J*-scrambling, vibrational relaxation, and the onset of liquid character

Journal:	*Physical Chemistry Chemical Physics*
Manuscript ID	CP-ART-07-2019-004101.R1
Article Type:	Paper
Date Submitted by the Author:	10-Sep-2019

Complete List of Authors:	Ng Pack, Greg; Boston University, Department of Chemistry; Boston University, Photonics Center Rotondaro, Matthew; Boston University, Department of Chemistry; Boston University, Photonics Center Shah, Parth; Boston University, Department of Chemistry; Boston University, Photonics Center Mandal, Aritra; University of Colorado Boulder, Department of Chemistry Erramilli, Shyamsunder; Boston University, Department of Physics; Boston University, Photonics Center Ziegler, Lawrence; Boston University, Department of Chemistry; Boston University, Photonics Center

Two-dimensional infrared spectroscopy from the gas to liquid phase: Density dependent *J*-scrambling, vibrational relaxation, and the onset of liquid character

Greg Ng Pack[1,3], Matthew C. Rotondaro[1,3], Parth P. Shah[1,3], Aritra Mandal,[4]

Shyamsunder Erramilli[2,3] and L.D. Ziegler[1,3*]

[1]Department of Chemistry, Boston University, Boston, MA 02215 USA
[2]Department of Physics, Boston University, Boston, MA 02215 USA
[3]Photonics Center, Boston University, Boston, MA 02215 USA
[4]Department of Chemistry, University of Colorado, Boulder CO 80309 USA

*Author to whom correspondence should be addressed: lziegler@bu.edu

MCR Orchid ID: 0000-0002-7707-7589
AM Orchid ID: 0000-0002-8680-3730

KEYWORDS: 2DIR, VER, supercritical fluids, rotational relaxation

Abstract

Ultrafast 2DIR spectra and pump-probe responses of the N_2O ν_3 asymmetric stretch in SF_6 as a function of density from the gas to supercritical phase and liquid are reported. 2DIR spectra unequivocally reveal free rotor character at all densities studied in the gas and supercritical region. Analysis of the 2DIR spectra determines that *J*-scrambling or rotational relaxation in N_2O is highly efficient, occurring in ~ 1.5 to ~2 collisions with SF_6 at all non-liquid densities. In contrast, N_2O ν_3 vibrational energy relaxation requires ~ 15 collisions, and complete vibrational equilibrium occurs on the ~ns scale at all densities. An independent binary collision model is sufficient to describe these supercritical state point dynamics. The N_2O ν_3 in liquid SF_6 2DIR spectrum shows no evidence of free rotor character or spectral diffusion. Using these 2DIR results, hindered rotor or liquid-like character is found in gas and all supercritical solutions for SF_6 densities $\geq \rho^* = 0.3$, and increases with SF_6 density. 2DIR spectral analysis offers direct time domain evidence of critical slowing for SF_6 solutions closest to the critical point density. Applications of 2DIR to other high density and supercritical solution dynamics and descriptions are discussed.

I. Introduction

Vibrational spectroscopic lineshapes in solutions encode a wealth of information about intermolecular interactions, energy relaxation rates, and the structure and dynamics of the surrounding solvent at a given state point. As a molecule's environment changes from that of a dilute gas to one whose density is characteristic of a liquid, rovibrational spectral shapes correspondingly evolve and thus report on these fundamental properties as a function of temperature, pressure and density. At low densities, where the solution is in the gas phase, vibrational spectra are characterized by discrete resolvable *P(J)* (ΔJ = -1) and *R(J)* (ΔJ = +1) rotational transitions and, when symmetry allowed, a *Q*-branch (ΔJ = 0).[1] Due to the spectral resolution, such systems can readily provide information about intermolecular collisions, the shapes of interaction potentials, coherent quantum dynamics and quantum specific energy decay. However, as the surrounding fluid's density increases, collisional broadening obscures the resolved discrete *J* rovibrational absorption features and *v, J* quantum specific information, such as the distinct timescales of rotational and vibrational relaxation, are not readily evident spectroscopically. As the fluid's density increases further and approaches liquid-like densities only vestigial evidence, at best, of the diffuse rotational branches can be detected in the IR spectrum and the nature of the lineshape becomes increasingly dependent on theoretical modeling.[2] At even higher densities, including state points in the supercritical region, bandshapes begin to narrow resembling their absorption spectral bandshapes in liquid solution. It is unclear if these nearly featureless spectra are due to quasi-free rotors, hindered rotational or librational transitions, or some dynamic combination of these. Experimental characterization of these fluid solutions, correspondingly as gas, liquid or a dynamic inhomogeneous mix, is thus limited.

The use of ultrafast 2DIR spectroscopy[3] to learn about rotational and vibrational relaxation in dense fluids, special solvation effects in the supercritical fluid (SCF) phase, and the evolution of liquid phase character, as a function of fluid density is reported here. Much of what is known about gas phase reaction dynamics has come from state-to-state, time-resolved spectroscopic measurements necessarily in relatively low density systems where discrete rotational spectroscopic features are resolvable.[4] However, dense fluids, particularly at high temperatures and pressures, are solvent environments important to many chemical processes. For example, internal combustion engines operate under high pressures, in the 5-100 atm range, and often in the supercritical regime.[5] Given the lack of spectral resolution largely due to quasi-elastic and inelastic collisional effects in

such high density/pressure fluids, echo-like spectroscopic techniques, such as 2DIR, are uniquely suited to uncover dynamical information on how excited molecules in these dense environments return to equilibrium with both *J* and *v* specificity.[6] Rates of chemical reactions are often controlled by how quickly excited or highly energetic species lose internal energy and return to rotational and vibrational thermal equilibrium. As demonstrated here, 2DIR offers a unique capability for learning about both rotational and vibrational relaxation as a function of fluid density and thus can thus be exploited to provide critical tests of our fundamental theoretical understanding of small molecule relaxation in dense chemical reaction environments.[7]

The unique and readily tunable solvation properties of SCFs offer the potential for controlling chemical processes.[8] Additional interest in SCFs has been especially peaked by the use of sc-CO_2 and sc-H_2O as potential inexpensive "green" solvents.[9-11] Enhanced local density effects have been indicated to play a role in the special solvation properties of SCFs and identified in simulations.[12-17] In addition, the slowing of density fluctuations, due to long range spatial correlations near the critical point, is also a dynamical characteristic of the critical point phase region.[18-21] Only a relatively few direct time-domain measurements of molecular responses in SCFs have been reported. These include some vibrationally resonant ultrafast pump-probe experiments.[22-26] Very dramatic effects near the critical point are generally not observed in these lifetime and transient absorption data, and most pump-probe responses follow the density dependence of trends both below and above the critical density (ρ_c). However, a faster lifetime (T_1) was observed for an IR active mode of $W(CO)_6$ in supercritical CO_2, C_2H_6, and CHF_3 at densities just below ρ_c than expected by simple phenomenological trends, and T_1 remained essentially constant for a range of densities around the critical point, ~$0.6\rho_c$ to ~$1.4\rho_c$, when the temperature was near T_c.[22,24] These near critical effects were reproduced by a theory based on mostly thermodynamic properties of the solvent, neglecting local enhancement effects, and achieved good agreement with observed density dependence.[23,24] However, 2DIR may provide a more direct experimental measure of anomalous fluctuation dynamics and inhomogeneities near a critical point than lifetime measurements because this spectroscopic approach provides a direct, experimental measure of the transition energy *fluctuation* dynamics. This study is the first 2DIR report of the real time fluctuation dynamics in SCF solutions.

Furthermore, although the supercritical region is traditionally described as exhibiting single phase character, i.e. no liquid, vapor distinction, some thermodynamic properties have

maxima where $P > P_c$ and $T > T_c$, and lines that connect these maxima have been used to distinguish gas and liquid like character in the SCF region. For example, a "Widom line" defined by the maxima of the constant pressure specific heat, or some other thermodynamic response functions, as a function of T extending from the critical point has served to divide the supercritical fluid into gas and liquid-like regions.[27-31] Another line dividing a supercritical fluid in two regions, a low-temperature "rigid" liquid and a high-temperature nonrigid gas-like fluid, the Frenkel line, has also been proposed.[32,33] Dynamics revealed by 2DIR may be expected to qualitatively change in supercritical regions where the Widom or Frenkel line boundaries can be identified and experimentally distinguish gas or liquid like supercritical regions.

As introduced above, a final aim of these studies is to learn how density dependent 2DIR measurements can reveal and identify the onset of liquid properties in supercritical and near-liquid density solutions and is made possible by our recent characterization of free rotor 2DIR spectra in low density solutions.[6] There is an extensive literature on the observation and molecular-level interpretation of the vibrational spectra of small molecules, especially IR absorption spectra of hydrogen halides in high pressure and simple non-polar liquids, that closely relates to this 2DIR analysis.[2,34-50] A characteristic phenomenological feature of these IR spectra is the observation of a broad and overlapping "triplet" structure for vibrational bands of diatomics in these liquids and high pressure fluids. The two feature or shoulders on the red and blue of the vibrational absorption band are attributed to unresolved P (ΔJ = -1) and R (ΔJ = +1) gas-phase-like rovibrational branches. The middle feature is close to the vibrational transition frequency observed in condensed phase FTIR spectra and suggests the interpretation of the center resonance as a Q-branch ($\Delta J = 0$). However, for all diatomics, and all parallel polarized vibrational bands, the Q-branch is strictly dipole symmetry-forbidden in free space[1,51] due to conservation of angular momentum constraints.

Despite the simplicity of these fluid solutions, various theoretical and computational approaches have been applied to understand the appearance of these observed complex IR absorption lineshapes, characterized by the density dependent triplet structure and Q-branch like absorption intensity in high density environments. Explanations offered for these diatomics in liquid and dense fluid vibrational bandshapes span the range from dipole-induced-dipole effects,[36] J-mixing due to anisotropic interaction potential,[37] van der Waals complex formation or long lived anisotropic spatial correlations in the fluid,[2,38,39,48] "modified rotor" or hindered rotor descriptions,[42,43,50] to P and R spectral interference effects.[49] Some analyses have speculated that

these complex lineshapes are due to both mixed free rotor character and modified rotor character resulting from slowly varying anisotropic solute-solvent potentials and the role of barriers on the lower lying rotational levels.[41,45-47] The obvious *experimental* feature that limits more detailed interpretation of the high fluid density rovibrational absorption spectra is the lack of resolved rotational features. Hence, these broad, relatively structureless diatomic vibrational features in liquids and dense fluids still remain open to a variety of interpretations. As demonstrated here (*vide infra*) 2DIR studies can provide greater insight into the origins of this complex lineshape behavior.

Over the past two decades ultrafast two-dimensional infrared (2DIR) spectroscopy has been shown to be a powerful time-domain technique for learning about nuclear dynamics in the condensed phase on the femto- to picosecond time scale.[3,52] Analysis of 2DIR spectra yields information on the nature of vibration lineshapes in terms of transition energy fluctuation dynamics and inhomogeneous broadening effects, the coupling of resonant intra- or intermolecular modes or the dynamics of chemical exchange between interconverting discrete molecular configurations or species.[53-57] This information is obtained by distributing the three-pulse vibrational response over a pump excitation frequency axis (ω_1) and a probe detection frequency axis (ω_3) as a function of T_w, the fixed time delay between the second and third pulse. Condensed phase coherent 2DIR spectra resonant with a single vibrational absorption exhibit two oppositely signed spectral features at the $0 \rightarrow 1$ and the $1 \rightarrow 2$ vibrational frequencies which respectively result from ground state bleach and stimulated emission (GSB-SE), and excited state absorption (ESA) signal polarization pathways. The GSB-SE polarization response is centered at the pure vibrational resonance along the diagonal ($\omega_1 = \omega_3$), and the corresponding ESA signal is red-shifted along the probe frequency axis ω_3 by the $1 \rightarrow 2$ anharmonicity. Molecular fluctuation timescales due to bath interactions in these condensed phase systems are determined by the waiting time (T_w) dependence of the 2DIR lineshapes and correspond to the transition frequency-frequency correlation function (FFCF) of a resonantly excited vibrational mode.[3]

While all previous ultrafast 2DIR studies spectra have been carried out for vibrators in condensed phase solutions, we have recently described the first corresponding 2DIR analysis of a quasi free quantum rotor.[6] The 2DIR spectra of the resonantly excited ν_3 asymmetric stretching rovibrational band (2220 cm^{-1}) of N_2O in SF_6 gas at two densities ($\rho^* = \rho/\rho_c = 0.16$ and 0.30; $\rho_c = 0.74$ g $mL^{-1} = 5.79$ M) showed a qualitatively different and considerably more complex spectral signature than seen for the 2DIR spectra of isolated vibrational resonances in condensed phases.

The N_2O ν_3 mode has strong oscillator strength (ε ~1.5 x 10^3 M^{-1} cm^{-1}) in a relatively transparent region of the mid-IR spectrum and a small dipole moment (0.16D) allowing it to act as an effective small molecule probe in a wide variety of solutions. In addition, the N_2O ν_3 mode is relatively long lived[58] (*vide infra*) thus enabling 2DIR fluctuation dynamics measurements for relatively long timescales, as seen below. SF_6 is a relatively simple, chemically inert, non-polar fluid with a readily accessible critical point (T_c = 45.6°C, P_c = 36.6 atm). At early waiting times spectral 'X' shapes, with diagonal and anti-diagonal spectral features, displaced by the ν_3 anharmonicity along the ω_3 axis identify 2DIR features attributable to ground state bleach and excited state absorption contributions to the N_2O 2DIR spectrum.[6] The elongated spectral shapes along the diagonal (centered at $\omega_1 = \omega_3 \sim \omega_{10}^R$ and $\omega_1 = \omega_3 \sim \omega_{10}^P$) and the parallel components red-shifted in the ω_3 direction (centered at $\omega_1 = \omega_3 \sim \omega_{21}^R$ and $\omega_1 = \omega_3 \sim \omega_{21}^P$) by the ν_3 $1 \rightarrow 2$ transition anharmonicity (~28 cm^{-1}) in the early time (T_w ~ 0.2 ps), are the well-known 2DIR signatures of an inhomogeneously broadened vibrational band. The corresponding anti-diagonal features (centered at $\omega_1 \sim \omega_{10}^R, \omega_3 \sim \omega_{10}^P$; $\omega_1 \sim \omega_{10}^P, \omega_3 \sim \omega_{10}^R$; $\omega_1 \sim \omega_{21}^R, \omega_3 \sim \omega_{21}^P$ and $\omega_1 \sim \omega_{21}^P, \omega_3 \sim \omega_{21}^R$) seen in these quasi-free rotor spectra are not observed in condensed phase and are the key spectral feature that identifies a population of free rotors in a 2DIR spectrum. The initial elongated features all approach symmetrical shapes at longer waiting times which is the well-known signature of transition frequency memory loss, the 2DIR spectral characteristic of spectral diffusion processes in liquid phase environments. The T_w dependence of these 2DIR spectra showed that ν_3 N_2O rotational relaxation occurred in ~1.5 collisions at both moderately dense ρ^* = 0.16 and 0.30 SF_6 environments (9.5 ps and 6.0 ps, respectively). The goal here is to extend these 2DIR measurements of N_2O's ν_3 band in higher densities of SF_6, including state points in the vicinity of the critical point and above, as well as in liquid SF_6 to learn about the density dependent rates of *J*-scrambling (rotational) and vibrational energy loss, relaxation in the critical point region and evidence of the onset of liquid-like character in this system. These nonlinear spectroscopic studies allow experimental tests of the adequacy of independent binary collision (IBC) relaxation models in dense fluids, determine how solute-solvent intermolecular properties separately influence rotational and vibrational relaxation, and characterize the transition from gas to condensed phase

dynamics, at high densities, where attributes of both solvation environments may be simultaneously present.

II. Experimental

Sample Preparation

N_2O (99.999%, Linde Gas) and SF_6 (99.8%, Airgas, Inc.) gases were compressed by a pressure generator (HiP 87-6-5) in an evacuated, high-pressure gas mixing set-up into a grade 316 stainless steel optical cell with a 100 μm thick PTFE (Teflon) spacer sandwiched between two 2 mm thick CaF_2 windows and sealed by Teflon O-rings. All N_2O/SF_6 solutions were allowed to equilibrate for ~24 hours before any spectroscopic measurements were performed to ensure complete mixing. The resulting solutions were set to a temperature near 48.0ºC to reach the desired state point using electrical rope heater completely wrapped around the cell (minimizing temperature gradients) and a K-type bolt-on thermocouple wire (WTK-10-60, OMEGA Engineering, Inc.) connected to a benchtop temperature controller (CSi32K-C24, OMEGA Engineering, Inc.). Proportional integral derivative (PID) control was used to regulate and maintain temperatures to within ±0.1°C. The pressure of the cell was detected by a thin film pressure transducer gage (PX603, OMEGA Engineering, Inc.) connected to a benchtop pressure meter (DP25B-S, OMEGA Engineering, Inc.) within a precision of ±1 psi. Relative sample densities were derived from the NIST online database.[59]

FTIR Spectra

Linear FTIR spectra were collected on a ThermoNicolet Nexus 670 FTIR spectrometer at 0.125 cm^{-1} resolution using Happ-Genzel apodization. The maximum FTIR absorbance of the N_2O ν_3 band was kept in the range of ~0.3-0.5 OD for all 2DIR measurements.

2DIR Spectra

A diode-pumped Legend Elite Duo (Coherent, Inc.) Ti:sapphire regenerative amplifier produces ultrafast pulses centered at 800 nm at a 1 kHz repetition rate with energies of 7.5 mJ/pulse, a pulse duration of 40 fs, and a bandwidth of 30 nm. The 800 nm output undergoes nonlinear down conversion through a TOPAS-C (Light Conversion) optical parametric amplifier (OPA) incorporating β-BaB_2O_4 (BBO) crystals to generate 1.3 and 1.8 μm signal and idler beams, respectively. Infrared pulses (10 μJ, 85 fs, 250 cm^{-1} FWHM) centered at 4.5 μm (~2222 cm^{-1}) are

produced by collinear combination of the OPA output beams in a difference frequency generation (DFG) $AgGaS_2$ crystal.

The 2DIR spectrometer is set up in a compact pump-probe geometry described elsewhere,[60] in which the two collinear pump beams are outputs of a modified Mach-Zender/Michelson interferometer, and the probe beam is a reflection off a 0.5º BaF_2 wedge. The IR beams are expanded and tightly focused onto the sample by a parabolic mirror to a focal spot diameter of ~100 μm. The phase-matched direction of the coherent, heterodyne-detected signal is in the probe direction. The heterodyned signal is dispersed in a monochromator (Princeton Instruments, Inc.) by a grating, and detected by a double-array 32 element MCT detector (InfraRed Associates, Inc.) with a resolution of 3 cm^{-1}/pixel. 2DIR spectra are collected in perpendicular polarization geometry <*XXYY*> in order to minimize scattering contamination to the 2DIR spectra.

Pump-probe responses

The one-color, pump-probe responses were obtained on the same 2DIR set-up with one of the pump beams blocked and is reported as the change in optical density ($\Delta OD(t)$) of the sample measured by the probe beam in the absence and presence of the pump beam, as a function of the interpulse delay time which is limited by our current scanning capabilities to 200 ps. The relative polarization of the pump and probe beams was set at the magic angle (54.7°) to eliminate orientational decay contributions to the pump-probe signals.

III. Results and Discussion

A. N_2O ν_3 absorption spectra as a function of SF_6 density

Normalized FTIR absorption spectra of the N_2O ν_3 asymmetric stretch in different SF_6 density solutions are shown in Fig. 1. These spectra highlight the continuous evolution of the ν_3 absorption lineshape from the gas to liquid phase. The $0 \rightarrow 1$ ν_3 excitation is a parallel polarized transition, and thus no Q-branch is formally allowed for the gas phase spectra.[1] Rotational fine structure is not evident in any of these spectra due to the broadening of the individual *P(J)* and R(*J)* discrete transitions. At the two lowest, gas-like SF_6 solvent densities shown here,[6] $\rho^* = 0.16$ (40˚C, 17 atm, $0.98T_c$, $0.46P_c$) and $\rho^* = 0.30$ (40˚C, 26 atm, $0.98T_c$, $0.71P_c$), *P* and *R* rovibrational branches are observed with easily resolvable peak maxima centered at 2211 cm^{-1} and 2236 cm^{-1}, respectively. In this modest density regime, the larger relative absorption in the "forbidden" *Q*-branch region (~2021 cm^{-1}) in the $\rho^* = 0.30$ spectrum (blue) is the most obvious difference.

As the SF_6 density increases further (Fig. 1), the *P* and *R* branches become progressively less distinct and absorption intensity grows in the ν_3 *Q*-branch region. *P* and *R* branch maxima are still identifiable in ρ^* = 0.67 (48˚C, 37.9 atm, 1.02T_c, 1.05P_c) and 0.86 (48˚C, 38.8 atm, 1.01T_c, 1.05P_c) solutions, and but become nearly indistinguishable at ρ^* = 0.99 (50˚C, 40.7 atm, 1.01T_c, 1.10P_c). At higher density, the vestige of *P* and *R* branches are barely evident as weak shoulders and the largest intensity is now in the *Q*-branch region as seen for the ρ^* = 1.36 (48˚C, 41.3 atm, 1.01T_c, 1.12P_c) fluid solution spectrum (Fig. 1). Note the ρ^* = 0.16 and 0.30 spectra are in the gas phase, and the ρ^* = 0.67, 0.86, 0.99 and 1.36 are all in the supercritical phase.

In contrast, the lineshape of the N_2O ν_3 in liquid SF_6 (ρ^*= 1.87, 20˚C, 22 atm, 0.92T_c, 0.60P_c) absorption spectrum is qualitatively different (Fig. 1). All vestiges of *P* and *R* branches are completely absent and a nearly Lorentzian band shape with a single peak frequency (2221 cm^{-1}) is observed for ν_3 in liquid SF_6 at ρ^*= 1.87. The small absorption feature at ~2207 cm^{-1} in this spectrum is due a bending ν_2 (589 cm^{-1}) hot band absorption ($\nu_2 \rightarrow \nu_2 + \nu_3$) as noted previously.[61,62] Interestingly, this small hot-band feature is only clearly evident for N_2O in liquid phase environments (SF_6, H_2O and octanol). The intensity of this feature relative to the fundamental ν_3 transition is highly solvent dependent, e.g. it is about 3 times bigger in octanol that H_2O.[62] The appearance of a small shoulder in the liquid but not the gas or supercritical SF_6 solutions is consistent with the solvent sensitivity of the transition moment of this absorption hot band. No rovibrational structure appears in any condensed phase N_2O ν_3 absorption spectrum.[61-65] Finally, in liquids, the N_2O ν_3 transition frequency is highly sensitive to solvent polarity.[65] The observed peak is at 2221 cm^{-1} in liquid SF_6 and only slightly red-shifted (2220 cm^{-1}) from that in the less dense supercritical SF_6 at ρ^* = 1.36 suggesting that this portion of the SCF spectrum results from a solvation environment similar to that of the liquid.

B. 2DIR spectra of N_2O ν_3 mode in dense gas and supercritical SF_6

2DIR spectra of the N_2O ν_3 mode in SF_6 at densities corresponding to the absorption spectra in Fig. 1 are shown in Fig. 2 as a function of some representative waiting times, T_w. These samples correspond to gas phase (ρ^* = 0.16) and supercritical state points, including state points near SF_6 ρ_c and approaching liquid density (ρ^* = 1.36). The "X" shape, most evident at early times in the ρ^* = 0.16 spectrum, fundamentally originates from the strict $\Delta J = \pm 1$ selection rule for each $\Delta\nu$ =

± 1 transition of a free rotor that contributes to the $P^{(3)}$ density matrix pathways contributing to the 2DIR signal response.[6] For an inhomogeneously broadened system, this leads to diagonal and the anti-diagonal "X" – like 2DIR features for an ensemble of quasi-free rotors at early T_w times for both GSB-SE and ESA contributions, as described earlier and evident in Fig. 2. The ESA contribution is red-shifted in the ω_3 direction by the N_2O ν_3 $1 \rightarrow 2$ transition anharmonicity (~28 cm^{-1}). Thus, any "X" like character in the 2DIR spectrum indicates quasi-free rotor character in the sample ensemble. The elongated shapes observed at the shorter T_w's result from the initial predominant inhomogeneous character of the ensemble of *J*-specific allowed rovibrational transitions.[6]

The underlying fluctuation dynamics of the system that determines the observed T_w dependence of these 2DIR spectra is captured by a stochastic Gaussian line broadening model.[66] Following the treatment of the 2DIR spectra for free rotors given previously,[6] lower density absorption spectra were modeled as separate transition frequency-frequency correlations (FFCF) given by the familiar Kubo lineshape formulism and centered on the *R* and *P* branch peaks:[66]

$$C_{1R,1R}(t) = \left\langle \delta\omega_{10}^{R}(t)\delta\omega_{10}^{R}(0) \right\rangle = +\Delta_{10}^{R}\Delta_{10}^{R}e^{-t/\tau_c} \qquad \text{(Eq. 1a)}$$

$$C_{1P,1P}(t) = \left\langle \delta\omega_{10}^{P}(t)\delta\omega_{10}^{P}(0) \right\rangle = +\Delta_{10}^{P}\Delta_{10}^{P}e^{-t/\tau_c} \qquad \text{(Eq. 1b)}$$

where $\omega_{10}^{P}(t) = \omega_{10}^{P^o} + \delta\omega_{10}^{P}(t)$ and $\omega_{10}^{R}(t) = \omega_{10}^{R^o} + \delta\omega_{10}^{R}(t)$, and $\omega_{10}^{P^o}$ ($\omega_{10}^{R^o}$) corresponds to the *P* (*R*) branch maximum. $\Delta_{10}^{P}, \Delta_{10}^{R}$ are the initial instantaneous widths of the corresponding $0 \rightarrow 1$ *P* and *R* rovibrational branches, and τ_c is the transition energy fluctuation time scale. In addition to these FFCF autocorrelations, a FFCF cross-correlation function is required to capture the structure and dynamics of the free rotor 2DIR spectra and its perfectly anticorrelated features:[6]

$$C_{1P,1R}(t) = C_{1R,1P}(t) = \left\langle \delta\omega_{10}^{P}(t)\delta\omega_{10}^{R}(0) \right\rangle = -\Delta_{10}^{P}\Delta_{10}^{R}e^{-t/\tau_c} \qquad \text{(Eq. 2)}$$

Changes in the aspect ratio of the elongated 2DIR spectral lineshapes as a function of T_w captures the decay of the FFCF.[67,68] The center line slope (CLS) method was used to quantify the T_w dependence of the initial elongated 2DIR features and thus the FFCF decay constant, τ_c.[67] The CLS at a given T_w is determined by the slope of the line that connects the maxima of the peaks of a series of cuts through the 2D spectrum parallel to the ω_1 frequency axis. τ_c is a measure of the

spectral diffusion dynamics or equivalently the timescale for *J*-specific initial transition frequency memory loss, *J*-scrambling, due to bath interactions.[6] More specifically, for these gas/fluid phase environments, it corresponds to the time for the excited rotational distribution to return to equilibrium as result of collisions of N_2O with the SF_6 solvent/bath.

The CLS determined FFCF for the diagonal and anti-diagonal GSB-SE components of the 2DIR spectra shown in Fig. 2 are also correspondingly plotted in this figure. Excellent exponential best-fits are obtained at each density. The CLS best-fit determined exponential rotational relaxation times, τ_c, as a function of SF_6 reduced density are summarized in Table 1. As noted in our earlier lower density report,[6] a very small (~5%) slow second FFCF component is found at all densities. This component provides a positive constant offset to the fitted CLS decays for *both* the diagonal and anti-diagonal 2DIR signal features, and may result from pure vibrational dephasing, sample heating or the cancelling effects of adjacent, oppositely signed 2DIR contributions. (2DIR and CLS decays for the $\rho^* = 0.86$ state point, 48°C, 38.8 atm, $1.00T_c$, $1.06P_c$, are shown in supplementary information for conciseness.)

Qualitative systematic trends are evident in the N_2O ν_3 2DIR spectra as a function of SF_6 density. At the lowest densities studied[6] ($\rho^* = 0.16$ and $\rho^* = 0.30$), eight distinct elongated signals are evident at early T_w times. Four contribute each to GSB-SE and ESA pathways, which carry different signed signals. However only four symmetrized features are evident at long times, where the FFCF is ≈ 0, because the N_2O ν_3 vibrational anharmonicity (28 cm^{-1}) almost exactly matches the frequency difference between *P* and *R* branch maxima (25 cm^{-1}) at the experimental temperatures (~40°C). Consequently the symmetrized diagonal GSB-SE contribution of the *P* transition almost exactly cancels the (*P*, *R*) ESA cross-peak, and the cross-peak (*R*, *P*) GSB-SE signals effectively cancel the ESA of the *R* transitions.[6]

In analogy to loss of distinct *P* and *R* branch structure in the FTIR spectra as the SF_6 density increases and described above (Fig. 1), the 2DIR spectra also exhibit less resolved rotational features with increasing SF_6 density. For example, the eight readily distinguished elongated feature at early times and four at long times evident at $\rho^* = 0.16$, are difficult or impossible to distinguish for the higher densities (Fig. 2). Cancellation of the overlapping diagonal *P* GSB-SE and ESA anti-diagonal (*P*, *R*) cross-peak, and the overlapping GSB-SE (*R*, *P*) cross-peak and ESA (*R*, *R*) features are already broadened at our shortest T_w at densities of $\rho^* = 0.67$ and higher so that this 2DIR spectral region shows no signal. However, the unique anti-diagonal 2DIR signature of free

rotor character *persists at all these dense gas and supercritical densities* thus allowing precise determination of *J*-scrambling or rotational relaxation times *even in the absence of any rotational resolution* in the corresponding linear spectra. This anti-diagonal 2DIR spectral structure in particular indicates some component of the resonant ensemble has free rotor character (Fig. 2). The T_w dependence of the collapse of the 2DIR anti-diagonal and diagonal structure provides this unique capability for studying rotational relaxation in high density fluids.

As the density or collision frequency increases from $\rho^* = 0.16$ to 1.36, a factor of 8.5 the timescale of rotational energy relaxation, τ_c, decreases from 9.4 ps to 1.35 ps, roughly a factor of 7. CLS decays of both the diagonal and anti-diagonal yield decays within the precision of these measurements. If we use calculated mean free times between N_2O and SF_6 collisions (τ_{coll}) based on hard sphere calculations (see SI), the number of collisions at each density that are required for N_2O to rotationally relax is given by $Z_{rot} = \tau_c/\tau_{coll}$. The 2DIR determined rotational relaxation times, τ_c and Z_{rot}, are plotted as a function of fluid density in Fig. 3a. As seen in the figure (and Table 1), rotational equilibration occurs within 1 to 2 collisions over this order of magnitude range of SF_6 fluid densities. Thus, as noted previously for the lowest density dense gas phase 2DIR analysis,[6] *J* memory loss due to collisions remains a highly efficient process in the supercritical region. The efficiency of rotational relaxation will be contrast with that of vibrational relaxation at these state points subsequently. The rate of rotational relaxation is nearly constant in this density region in terms of Z_{rot}, the number of SF_6 collisions to achieve rotational equilibrium, and thus the independent binary collision model is adequate for describing the relaxation dynamics at all these supercritical and gas state points. However, the data suggests there may be a small slowing effect at $\rho^* = 0.99$ (Z_{rot} maximum) or a small plateau in this region as the critical density is approached ($\sim\rho^* = 0.86$ to 0.99). This feature is better seen by plotting the fluctuation rate ($1/\tau_c$) as a function of density (Fig. 3b). The dashed straight line, extending from the origin, consistent with an IBC description, to the $\rho^* = 1.36$ rate, is a visual aid highlighting the fluctuation slowing in the critical point region. This density dependent data is consistent with critical fluctuation slowing effect and a potential plateau region in the critical point region. This effect is analogous to the $W(CO)_6$ lifetime effects in the same supercritical phase region of other fluids and is consistent with the analysis and conclusions of those SCF studies.[22-24,69]

C. 2DIR spectra of N_2O ν_3 mode in liquid SF_6.

The 2DIR spectrum of the N_2O ν_3 mode in liquid SF_6 (ρ^* = 1.87 at 20°C, 22 atm, 0.92T_c, 0.60P_c) is shown in Fig. 4 for T_w = 0.2 and 1.0 ps. Unlike the 2DIR N_2O in SF_6 spectra in gas and supercritical phase state points, no anti-diagonal features can be detected in the 2DIR of ν_3 in the liquid SF_6 environment even at the earliest T_w (0.2 ps). Thus, in contrast to the lower density fluids, no evidence of N_2O free rotor character can be detected in the liquid SF_6 2DIR spectra at this state point. This is consistent with the linear absorption spectrum where no vestiges of rotational branches can be detected (Fig. 1).

Furthermore, the spectrum is already fully symmetrized by 0.2 ps and no meaningful 2DIR shape changes are detected as a function of T_w (Fig. 4). This 2DIR spectrum characterizes a vibrational feature dominated by a single homogeneous dephasing time lacking any inhomogeneous character or spectral diffusion, at least at the limit of current IR pulse durations. The decay dynamics of the relevant FFCF for this N_2O mode at this solution state point, $\tau_c << 0.2$ ps, is consistent with the observed near Lorentzian character of the observed vibrational absorption lineshape (Fig. 1, and SI). The rapid fluctuation FFCF dynamics of the N_2O ν_3 mode in liquid SF_6 stands in contrast to photon echo results for N_2O solvated in octanol or water where significantly slower fluctuation processes are found, for example due to hydrogen bonding or alkyl chain dynamics, and instantaneous vibrational frequency memory loss occurs on much longer timescales.[62] This highlights the sensitivity of 2DIR and related ultrafast nonlinear spectroscopic technique to report on the chemical origins of solvation effects.

D. Estimates of non-free rotor N_2O character in FTIR as a function of SF_6 density.

All 2DIR spectra unequivocally show free rotor character at the investigated SF_6 non-liquid state points. These results can be used to provide experimental evidence for understanding the observed density dependent absorption spectra (Fig. 1) and the onset of liquid character in these systems. Extensions of these results to the long-studied triplet structure and anomalous *Q*-branch intensity for solutions of hydrogen halides in simple liquids follow as well. As demonstrated previously,[6] the N_2O ν_3 absorption spectra at the lowest densities studied here are phenomenologically well fit by a stochastic Gaussian line broadening model. Each *P* and *R* branch envelope is represented by Kubo lineshape functions only requiring $\Delta_{10}^{P}, \Delta_{10}^{R}$ and τ_c (Eq. 1a, b). Analysis of the 2DIR determines the fluctuation time scale, τ_c, due to N_2O-SF_6 collisions at each

density. Given this experimental value of τ_c, best fits to the observed $\rho^* = 0.16$ and 0.30 absorption spectra determined $\Delta_{10}^P, \Delta_{10}^R$. Excellent fits to the FTIR were obtained except in the spectral wings which is to be expected given the non-Gaussian character of the *P* and *R* branch spectral shapes in those spectral regions.[6] If we assume the distribution of initial, instantaneous *J* transition frequencies, which are mostly determined by rotational constants and temperature, $\Delta_{10}^P, \Delta_{10}^R$, is essentially unchanged as the fluid density increases, then the 2DIR determined τ_c values (Table 1) allow the calculation of the corresponding free rotor N_2O ν_3 absorption spectrum at each SF_6 density. The Gaussian widths for the *P* and *R* branch *J* transitions were found to be 21.4 cm^{-1} and 17.7 cm^{-1}, respectively, resulting from the best fits to lowest density $\rho^* = 0.16$ absorption spectrum using the corresponding 2DIR CLS decay result for τ_c (9.4 ps).

The calculated free rotor spectrum, using the fluctuation times, τ_c, obtained from the 2DIR spectral analysis, i.e. CLS decay, at each SF_6 density > 0.16 and the low pressure $\Delta_{10}^P, \Delta_{10}^R$ widths are shown (red line) in Fig. 5. These free-rotor spectra are compared to the observed FTIR spectra (blue line) at each density in this figure as well. This lineshape comparison reveals that the intensity in the *Q*-branch region cannot be captured by the free rotor absorption character as the density increases. To better estimate how the non-free rotor character in the *Q*-branch region is increasing with density, the calculated spectrum has been subtracted from the experimental one with the relative scaling determined so that the rotor contribution is as large as possible without resulting a negative difference spectrum. The difference spectrum in the *Q*-branch region is the blue shaded area in Fig. 5. Again, we are ignoring the difference spectrum in the absorption wings of the vibrational band where this modeling is not quantitative due to the Gaussian frequency distribution inherent to this lineshape model.[6] Despite this limitation far from the band center, this model succeeds in providing a 2DIR based interpretation of the most salient features of the experimental absorption spectra. The blue shaded portion of the difference spectra represents the forbidden "*Q*-branch" region spanning the range from ~2211-2236 cm^{-1} with a peak at ~2221 cm^{-1}, the liquid density peak frequency. This absorption component increases with density in the range as the system change from the more gas-like modest density environment to the more liquid-like higher density supercritical environment.

The resulting interpretation of the above analysis, based on the 2DIR results, is that there are simultaneously two types of N_2O molecules in the ensemble that contribute to the absorption spectra in high density SF_6 fluids in this spectral region; one is a free rotor gas phase species and the other is a hindered or liquid like solvated species. This spectral analysis neglects any interconversion dynamics between the two types of solvated N_2O molecules and can be described as an additional static inhomogeneity contributing to the FTIR. Once the solvent condenses, no free rotor population remains, as seen for the SF_6 liquid absorption and 2DIR, and vibrators can be best characterized by a rotational diffusive or librational response. The hindered/solvated rotors component accounts for the "*Q*-branch" type absorption features in this high fluid density as pictured in Fig. 6. Heuristically, the ratio of free rotor to liquid-like population contributing to the ν_3 spectroscopic features, $P_{rot/liq}(\rho)$, may be given by an Arrhenius type of expression describing the probability that a N_2O rovibrational level passes over a slowly varying, local density dependent SF_6 barrier, $E_{bar}(\rho)$:

$$P_{rot/liq}(\rho) \propto \exp\left(-\frac{E_{bar}(\rho)}{E_{rot}(J)}\right) \tag{3}$$

For low densities, $E_{bar}(\rho) \sim 0$, $P_{rot/liq}(\rho) \sim 1$ and the system is all free rotors showing *P* and *R* branch structure only, as for example in the $\rho^* = 0.16$ sample. For the liquid limit $E_{bar}(\rho) \sim \infty$, $P_{rot/liq}(\rho) \sim 0$ and only a more liquid-like, hindered rotor *Q* branch spectrum is observed, i.e. the $\rho^* = 1.87$ sample. At a specific density in between these two limits, $E_{bar}(\rho) \sim kT$ and thus the more rotationally and translationally energetic N_2O molecules are above the barrier and result in the sub-ensemble that accounts for the free rotor spectrum. Such an explanation was proposed for the absorption spectrum of HCl in near and supercritical SF_6.[46] The presence of the *Q* branch-like feature in the absorption spectra of N_2O in SF_6, made possible by this 2DIR analysis (Fig. 5), is a key experimental attribute signifying the onset of liquid-like character in the fluid that coexists with free rotors at a given state point. Thus the sample is spectroscopically inhomogeneous not just due to the distribution of barrier heights or solvation environments but, at a given solvation environment or spatial location, the molecular distribution of rotational energy relative to the barrier size will also result in sub-ensembles of free rotor or hindered rotor spectral signatures.

E. N_2O ν_3 vibrational energy relaxation as a function of SF_6 density.

To contrast the 2DIR rotational dynamics given by the CLS decays with the timescale of the N_2O ν_3 vibrational energy relaxation, magic angle, one-color pump-probe measurements for each of the SF_6 solutions studied here were carried out. The density-dependence and relative collision efficiency of these vibrational energy relaxation (VER) rates can be compared with the *J*-scrambling spectral diffusion dynamics revealed by the 2DIR analysis. Furthermore, the effects of the supercritical and liquid SF_6 environments on N_2O ν_3 VER may be contrasted with that of moderately dense gas phase.

The magic angle, one-color, pump-probe responses of the ν_3 $\nu = 1$ excited state of N_2O in SF_6 for all the state points studied here are shown in supplementary information. To avoid complications due to overlapping GSB-SA and ESA contributions, the $\Delta OD(t)$ signal integrated over ~30 cm^{-1} of the dispersed pump-probe signal, centered at 2240 cm^{-1} of the ν_3 rovibrational band, are reported here. A bi-exponential decay is observed for all the ν_3 N_2O in SF_6 pump-probe responses regardless of solution phase; gas, supercritical and liquid. In order to most accurately determine vibration relaxation rates and rationalize this biexponential decay character, the following VER mechanism and corresponding kinetic scheme is proposed. Due to the low density of states for this triatomic in the asymmetric stretch region, collisions are required for the dissipation of vibrational energy in these N_2O/SF_6 solutions. The highest frequency fundamental in SF_6 is the 948 cm^{-1} asymmetric stretching mode and it is mismatched with the N_2O ν_3 energy by ~ 1270 cm^{-1}. Thus the most rapid vibrational decay pathway minimally involves two receiving modes.[70] Vibrational levels contributing to the proposed ν_3 VER mechanism and biexponential pump-probe signal are diagramed in Fig 7. (00^00), (10^00), (00^01), (10^01), and (00^02) correspond to the ground, symmetric stretch, asymmetric stretch, symmetric-asymmetric stretch combination ($\nu_1+\nu_3$), and asymmetric stretch overtone of N_2O, respectively. The red vertical lines correspond to allowed dipole transitions within the pump/probe pulse bandwidth, and $\sigma_{002,001}$, etc. are the absorption cross-sections for the (00^01) $\rightarrow$ (00^02), etc. transitions.

Since the energy level gap (~940 cm^{-1}) between the excited N_2O ν_3 (00^01) at ~2220 cm^{-1} and ν_3 symmetric stretch (10^00) center at ~1285 cm^{-1} effectively matches the SF_6 ν_3 asymmetric stretching mode at 948 cm^{-1} (Fig. 7), the fastest decay component in the pump-probe response and the rate of N_2O ν_3 vibrational loss is attributed to resonant V $\rightarrow$ V collisional energy exchange

resulting in the excitation of the SF_6 ν_3 and the N_2O ν_1 modes. Vibrational relaxation redistribution through V → V processes is relatively rapid compared to V → T/R and is generally the first step in the VER of polyatomic systems.[71-73] The second, slower component observed in the one-color pump-probe responses is attributed to the dipole allowed N_2O $(10^00) \rightarrow (10^01)$ absorption, which falls in the frequency width of our probe pulse and consequently the second *ΔOD(t)* decay component reflects the longer lifetime of the symmetric stretch level (10^00).

Rate equations for this one-color N_2O ν_3 pump-probe response in SF_6 corresponding to mechanism discussed above and illustrated by the energy level diagram in Fig. 7 are given in the supplementary information. The corresponding normalized pump-probe signal at delay time t is given by:

$$\Delta OD(t) = C_1 e^{-k_1 t} - C_2 \left(\frac{k_1}{k_1 - k_2} e^{-k_1 t} - \frac{k_1}{k_1 - k_2} e^{-k_2 t} \right) \quad \text{(Eq. 4)}$$

where C_1 and C_2 are proportional to the $(00^00) \rightarrow (00^01)$ and $(10^00) \rightarrow (10^01)$ absorption cross sections respectively, and k_1 and k_2 are the inverse lifetimes of the ν_3 and ν_1 N_2O states respectively. Excellent fits to this kinetic model are obtained at all densities including the SF_6 liquid. See SI for a representative best-fit to the ν_3 resonant pump-probe response in $\rho^* = 0.86$ SF_6 and the component kinetics for the ν_3 vibrational energy relaxation and the subsequent ν_1 population build up. The coefficients and lifetimes determined by best fits of Eq. 4 to the observed pump-probe responses at a given solution density (ρ^*) are summarized in Table 2.

The relative absorption strengths, $C_1 / C_2 \approx 2$ at each state point, including the liquid, is consistent with the kinetic mechanism illustrated in Fig. 7. The vibrational lifetimes of the ν_3 vibrational energy decay ($\tau_1 = 1/k_1$) and $Z_{vib} = \tau_1/\tau_{coll}$, the ν_3 lifetimes in terms of number of hard sphere collisions at each dense gas and supercritical state point, in analogy to the plot of rotational relaxation times (Fig. 3a), are shown in Fig. 8. Just as found for the rotational relaxation rate, the vibrational relaxation rate increased by nearly an order of magnitude as density increased in the $\rho^* = 0.16$ to 1.36 range and effectively scaled with the number of SF_6 collisions (Fig. 8). That is, regardless of the density in this regime $Z_{vib} \approx 14$ thus again supporting an independent binary collision description for the dynamics at these state points. However, for rotational relaxation (τ_c) $Z_{rot} \approx 1.5 - 2$ as described above for this solute-bath

system. Thus, the 2DIR results reveal that SF_6 collisions are a factor of ~10 more efficient at relaxing rotational energy in the ν_3 excited fundamental level. However, while rotational equilibrium is re-established < 10 ps after excitation depending on the density, complete vibrational cooling, returning the system to vibrational equilibrium, occurs on the ~ ns timescale (Table 2) in this $SF_6 - N_2O$ system.

The slower *ΔOD(t)* decay time scale, τ_2 ($1/k_2$), is ~ 30 - 40 times slower than τ_1. The current 200 ps range of our pump-probe delay limits the precision of the reported τ_2, the lifetime of the N_2O symmetric stretch fundamental (10^00). The vibrational energy level structures of the $N_2O - SF_6$ collision partners (Fig. 7) accounts for the difference of these two decay rates. Unlike the proposed mechanism for N_2O vibrational relaxation from (00^01) to (10^00), there is no single SF_6 vibrational level resonant with the N_2O ν_1 energy so its relaxation to the ground state is governed by a higher process requiring three receiving modes, and hence the ~ 30 - 40 times slower VER rate for this ν_1 component of the *ΔOD(t)* decay.[70,74] At $\rho^* = 0.99$, the second decay component appears to be slower than the corresponding ν_1 energy relaxation rate at $\rho^* \sim 0.86$ or 1.36. This may be attributed to critical point dynamical effects, however, given the 200 ps limit of our pump-probe, we leave further comment on these slower dynamics to a subsequent study.

IV. Conclusions

Data are presented demonstrating that ultrafast 2DIR, when combined with conventional pump-probe spectroscopy, can be an effective tool for measuring the distinct rates of excited state rotational and vibrational relaxation for small molecules in high density gases and supercritical fluids where no discrete rovibrational resolution is evident in the corresponding linear absorption spectrum. In particular, the observation of anti-diagonal features in the 2DIR spectrum unequivocally identifies free rotor character in the molecular ensemble and is evident in the 2DIR for all the dense gas and supercritical state points examined here, $0.16 \leq \rho^* \leq 1.37$. For the N_2O ν_3 fundamental in SF_6, rotational energy equilibration occurs in 1 – 2 collisions at each state point from the dense gas to the supercritical fluid region, and thus rotational equilibration is a highly efficient process across all these density state points in this fluid system. In contrast, ν_3 vibrational energy loss is an order of magnitude slower than *J*-scrambling at each corresponding density, requiring ~14 SF_6 collisions to achieve VER and complete equilibration of vibrational energy occurs on the ~ ns timescale. Furthermore, these results establish that an IBC description appears

sufficient to describe the solvation dynamics in the gas and supercritical regime studied for this system. The validity of this simple IBC description will be tested by 2DIR studies at higher SF_6 SCF densities than 1.36, the effect of temperature on CLS decays and 2DIR measurements in other high density gas/supercritical systems. Unlike the supercritical fluid solutions however, the 2DIR of N_2O in liquid SF_6 ($\rho^* = 1.87$) shows no free rotor character and the ν_3 absorption lineshape is in the rapid fluctuation limit described by a FFCF with a fluctuation timescale << 0.2 ps.

The 2DIR determined time scale for rotational equilibration, Z_{rot} 1-2 N_2O-SF_6 collisions at all fluid densities is consistent with previously reported rates of rotation-to-translation energy transfer near room temperature where typically 1–10 collisions suffice for rotational relaxation.[75,76] Interestingly, $Z_{rot} \sim 1.3 - 2$ was estimated for (neat) N_2O vapor from ultrasonic measurements in agreement with the more direct ultrafast 2DIR results in dense SF_6 despite ~10^5 difference in fluid density.[77] Traditional techniques for measuring rotational relaxation dynamics[76] include different versions of pump-probe spectroscopy,[78-80] resonance fluorescence,[81] shock wave analysis[82] and ultrasonic absorption.[77,82-84] However, these techniques are restricted to low pressure regimes unlike the 2DIR methodology which can report on rotational relaxation dynamics in high temperature and pressure regions of phase space as shown here.

For the wide range of densities studied here ($\rho^* = 0.16 - 1.87$), the N_2O ν_3 rovibrational total bandwidth, including the liquid state point, decreases by just a factor of ~2 (Fig. 1). However, 2DIR reveals fluctuation dynamics that decrease more than 50 fold (~10 ps to < 0.2 ps) across this density range. This largely results from the strongly inhomogeneous character of this rovibrational system and is another illustration of the power of 2DIR spectroscopy to uncover dynamics completely hidden in absorption spectra and this nonlinear approach will be widely applicable to other dense fluid systems.

In addition to establishing free rotor character in these dense fluids, the 2DIR analysis (CLS determined τ_c) provides an experimental estimate for coexisting liquid-like character. This component, contributing to intensity in the gas-phase forbidden *Q*-branch region of the linear absorption spectrum, increases with density. Thus, in these dense gas and supercritical SF_6 solutions, 2DIR experiments are consistent with the description that N_2O has simultaneous free rotor and hindered rotor subpopulations, and this heterogeneity results, in part, from the distribution of rotational energies relative to the density dependent N_2O-SF_6 potential barriers heights. As the density increases, the average effective barrier heights increase and a larger portion

of the entire ensemble has insufficient rotational energy to exceed these barrier energies. Subsequent isobaric temperature studies for a number of pressures and simulations will be carried out to develop more quantitative description of the heuristic barrier model (Eq. 3).

This growing intensity in the nominally forbidden gas phase *Q*-branch region is phenomenologically analogous to the triplet structure previously observed in the numerous studies of the absorption spectra of hydrogen halides in nonpolar liquids.[2,34-50] 2DIR studies of these diatomics in these dense nonpolar fluids can also establish the free rotor character in these diatomic probe systems and their state point dependence. MD simulations and calculations have been carried out to understand the origins of these absorption spectra and what they reveal about solvation in the liquid and high-pressure environments. Re-examining these systems with the quantitative fluctuation dynamics provided by 2DIR measurements would provide a better understanding of this long studied phenomenon and the gas to liquid solvation transition in these systems (and others).

An advantage of 2DIR relative to some other time domain techniques is that CLS decays directly report on bath fluctuation dynamics, at least as they couple to the reporting probe molecule's (ro)vibrational energy. A modest slowing of the fluctuation dynamics appears in SF_6's critical point region. This observation is analogous to the faster vibrational lifetimes found for $W(CO)_6$ in SCF solutions at densities near the critical point region.[22-24] However, in 2DIR, as shown here, such critical *slowing* effects are directly observed in contrast to being inferred from T_1 effects. 2DIR measurements in our lab are ongoing to map this critical slowing effect with greater precision in the N_2O-SF_6 system.

As these results demonstrate, 2DIR can establish the relative amounts of gas or liquid like character at all phase points in the supercritical region when the corresponding absorption character is devoid of any rotational structure. In contrast to previous studies[27-33] which have generally relied on simulation results to test the concept of Frenkel or Widom lines to demarcate regions in the supercritical region with dominate liquid or gas like structure, 2DIR can be an effective experimental tool for this purpose and test the validity of these concepts in the SCF region in general. In another potential application, 2DIR can be used to study the dynamics of small molecules photoproducts in dense fluids (gas, supercritical and liquid) as these excited fragments return to equilibrium even when rotational features are not resolved. For example, a transient absorption study of the rotational cooling of hot CN resulting from BrCN photodissociation in

perfluorohexane was recently reported.[7] The rovibrational band of this diatomic showed no rotational resolution and thus the analysis of the cooling of this degree of freedom relied on best fit modeling results including both free-rotor (*P, R*) and hindered rotor (*Q*-branch) contributions. 2DIR spectroscopy has the capacity to quantitatively provide measurements or rotational relaxation for such systems as shown here.

Acknowledgement

This material is based upon work supported by the National Science Foundation under CHE – 1609952.

Table 1. Rotational equilibration times determined by 2DIR CLS decay times (τ_c) and number of collisions ($Z_{rot} = \tau_c/\tau_{coll}$) as a function of SF_6 reduced densities in the gas and supercritical phases.

SF_6 density[a]	τ_c /ps[b]	τ_{coll} /ps	$Z_{rot} = \tau_c/\tau_{coll}$
$\rho^* = 0.16$[6]	9.5 ± 0.5	7.0	1.4
$\rho^* = 0.30$[6]	6.0 ± 0.4	3.8	1.6
$\rho^* = 0.67$	2.8 ± 0.3	1.7	1.6
$\rho^* = 0.86$	2.4 ± 0.2	1.3	1.8
$\rho^* = 0.99$	2.3 ± 0.2	1.1	2.0
$\rho^* = 1.36$	1.4 ± 0.3	0.8	1.8

[a]Density given in reduced density units relative to SF_6 critical point density: $\rho^* = \rho/\rho_c$
[b]Average of diagonal and antidiagonal CLS decay constants.

Table 2. N_2O ν_3 VER kinetics determined by fits to a bi-exponential fit to ΔOD responses.*

	$\rho^* = 0.16$[6]	$\rho^* = 0.30$[6]	$\rho^* = 0.86$	$\rho^* = 0.99$	$\rho^* = 1.36$	$\rho^* = 1.87$
C_1/C_2	2.0	1.9	1.8	1.8	1.8	1.8
τ_1 /ps	102 ± 10	34 ± 15	20 ± 3	17 ± 6	11 ± 3	6 ± 1
τ_2 /ps	≫ 1000	> 1000	590 ± 130	> 1000	490 ± 80	200 ± 20

*Precision estimates given by determining the limits of the two lifetimes, τ_1 and τ_2, for which the sum of squared residuals (SSR) are ≤ 1.5 × that of the best fit, such that a systematic distribution of residuals was not observed.

References

(1) Herzberg, G. *Infrared and Raman Spectroscopy of Polyatomic Molecules*; Van Nostrand: New York, 1954.

(2) Burshtein, A. I.; Temkin, S. I. *Spectroscopy of Molecular Rotation in Gases and Liquids*; Cambridge University Press: Cambridge, 1994.

(3) Hamm, P.; Zanni, M. T. *Concepts and Methods of 2D Infrared Spectroscopy*; Cambridge, 2011.

(4) Cheo, P. K.; Abrams, R. L. *Applied Physics Letters* **1969**, *14*, 47.

(5) Foster, J.; Miller, R. S. In *High Pressure Processes in Chemical Engineering*; Lackner, M., Ed.; ProcessEng Engineering GmbH: 2010, p 53.

(6) Mandal, A.; Ng Pack, G.; Shah, P. P.; Erramilli, S.; Ziegler, L. D. *Physical Review Letters* **2018**, *120*, 103401.

(7) Grubb, M. P.; Coulter, P. M.; Marroux, H. J. B.; Hornung, B.; McMullen, R. S.; Orr-Ewing, A. J.; Ashfold, M. N. R. *Nature Chemistry* **2016**, *8*, 1042.

(8) Kajimoto, O. *Chemical Reviews* **1999**, *99*, 355.

(9) DeSimone, J. M. *Science* **2002**, *297*, 799.

(10) Leitner, W. *Accounts of Chemical Research* **2002**, *35*, 746.

(11) Peach, J.; Eastoe, J. *Beilstein J. Org. Chem.* **2014**, *10*, 1878.

(12) Maddox, M. W.; Goodyear, G.; Tucker, S. C. *The Journal of Physical Chemistry B* **2000**, *104*, 6248.

(13) Heitz, M. P.; Bright, F. V. *The Journal of Physical Chemistry* **1996**, *100*, 6889.

(14) Song, W.; Biswas, R.; Maroncelli, M. *The Journal of Physical Chemistry A* **2000**, *104*, 6924.

(15) Wada, N.; Saito, M.; Kitada, D.; Smith, R. L.; Inomata, H.; Arai, K.; Saito, S. *The Journal of Physical Chemistry B* **1997**, *101*, 10918.

(16) Tucker, S. C. *Chemical Reviews* **1999**, *99*, 391.

(17) Tucker, S. C.; Maddox, M. W. *The Journal of Physical Chemistry B* **1998**, *102*, 2437.

(18) Maddox, M. W.; Goodyear, G.; Tucker, S. C. *The Journal of Physical Chemistry B* **2000**, *104*, 6266.

(19) Heitz, M. P.; Maroncelli, M. *The Journal of Physical Chemistry A* **1997**, *101*, 5852.

(20) Goodyear, G.; Tucker, S. C. *The Journal of Chemical Physics* **1999**, *111*, 9673.

(21) Das, M.; Green, J. R. *Nature communications* **2019**, *10*, 2155.

(22) Urdahl, R. S.; Myers, D. J.; Rector, K. D.; Davis, P. H.; Cherayil, B. J.; Fayer, M. D. *The Journal of Chemical Physics* **1997**, *107*, 3747.

(23) Myers, D. J.; Shigeiwa, M.; Fayer, M. D.; Cherayil, B. J. *Chemical Physics Letters* **1999**, *313*, 592.

(24) Myers, D. J.; Shigeiwa, M.; Fayer, M. D.; Cherayil, B. J. *The Journal of Physical Chemistry B* **2000**, *104*, 2402.

(25) Schwarzer, D.; Lindner, J.; Vöhringer, P. *The Journal of Physical Chemistry A* **2006**, *110*, 2858.

(26) Czurlok, D.; von Domaros, M.; Thomas, M.; Gleim, J.; Lindner, J.; Kirchner, B.; Vohringer, P. *Physical Chemistry Chemical Physics* **2015**, *17*, 29776.

(27) Simeoni, G. G.; Bryk, T.; Gorelli, F. A.; Krisch, M.; Ruocco, G.; Santoro, M.; Scopigno, T. *Nature Physics* **2010**, *6*, 503.
(28) Gallo, P.; Corradini, D.; Rovere, M. *Nature Communications* **2014**, *5*, 5806.
(29) Xu, L.; Kumar, P.; Buldyrev, S. V.; Chen, S. H.; Poole, P. H.; Sciortino, F.; Stanley, H. E. *Proceedings of the National Academy of Sciences of the United States of America* **2005**, *102*, 16558.
(30) Hestand, N. J.; Strong, S. E.; Shi, L.; Skinner, J. L. *The Journal of Chemical Physics* **2019**, *150*, 054505.
(31) Gorelli, F. A.; Bryk, T.; Krisch, M.; Ruocco, G.; Santoro, M.; Scopigno, T. *Scientific Reports* **2013**, *3*, 1203.
(32) Brazhkin, V. V.; Fomin, Y. D.; Lyapin, A. G.; Ryzhov, V. N.; Tsiok, E. N.; Trachenko, K. *Physical Review Letters* **2013**, *111*, 145901.
(33) Fomin, Y. D.; Ryzhov, V. N.; Tsiok, E. N.; Brazhkin, V. V. *Physical Review E* **2015**, *91*, 022111.
(34) Bulanin, M. O.; Orlova, N. D. *Opt. Spectrosc.* **1958**, *4*.
(35) Turrell, G. C.; Vu, H.; Vodar, B. *The Journal of Chemical Physics* **1960**, *33*, 315.
(36) Kwok, J.; Robinson, G. W. *The Journal of Chemical Physics* **1962**, *36*, 3137.
(37) Goldring, H.; Kwok, J.; Robinson, G. W. *The Journal of Chemical Physics* **1965**, *43*, 3220.
(38) Bratož, S.; Martin, M. L. *The Journal of Chemical Physics* **1965**, *42*, 1051.
(39) Robert, D.; Galatry, L. *Chemical Physics Letters* **1967**, *1*, 399.
(40) Perez, J.; Velasco, S.; White, J. A.; Hernández, A. C. *Journal of Molecular Liquids* **1990**, *45*, 71.
(41) Medina, A.; Roco, J. M. M.; Calvo Hernández, A.; Velasco, S.; Bulanin, M. O.; Herrebout, W. A.; van der Veken, B. J. *The Journal of Chemical Physics* **2002**, *116*, 5058.
(42) Medina, A.; Roco, J. M. M.; Calvo Hernández, A.; Velasco, S. *The Journal of Chemical Physics* **2003**, *119*, 5176.
(43) Medina, A.; Roco, J. M. M.; Calvo Hernández, A.; Velasco, S. *The Journal of Chemical Physics* **2004**, *121*, 6353.
(44) Medina, A.; Roco, J. M. M.; Hernández, A. C.; Velasco, S. *The Journal of Chemical Physics* **2005**, *123*, 234509.
(45) Bulanin, M. O.; Kerl, K.; Padilla, A.; Hernández, A. C.; Pérez, J. *Physical Chemistry Chemical Physics* **2003**, *5*, 285.
(46) Padilla, A.; Pérez, J.; Kerl, K.; Bulanin, M. O. *Journal of Molecular Structure* **2003**, *651-653*, 561.
(47) Pérez, J.; Padilla, A.; Herrebout, W. A.; Van der Veken, B. J.; Hernández, A. C.; Bulanin, M. O. *The Journal of Chemical Physics* **2005**, *122*, 194507.
(48) Padilla, A.; Pérez, J.; Herrebout, W. A.; Van der Veken, B. J.; Bulanin, M. O. *Journal of Molecular Structure* **2010**, *976*, 42.
(49) Padilla, A.; Pérez, J. *The Journal of Chemical Physics* **2013**, *139*, 084505.
(50) Padilla, A.; Pérez, J. *Journal of Molecular Spectroscopy* **2015**, *316*, 22.
(51) Herzberg, G.; Herzberg, L. *The Journal of Chemical Physics* **1950**, *18*, 1551.
(52) Cho, M. *Chemical Reviews* **2008**, *108*, 1331.
(53) Fayer, M. D.; Moilanen, D. E.; Wong, D.; Rosenfeld, D. E.; Fenn, E. E.; Park, S. *Accounts of chemical research* **2009**, *42*, 1210.

(54) Roberts, S. T.; Ramasesha, K.; Tokmakoff, A. *Accounts of chemical research* **2009**, *42*, 1239.
(55) Ramasesha, K.; De Marco, L.; Mandal, A.; Tokmakoff, A. *Nature chemistry* **2013**, *5*, 935.
(56) Schmitz, A. J.; Hogle, D. G.; Gai, X. S.; Fenlon, E. E.; Brewer, S. H.; Tucker, M. J. *J Phys Chem B* **2016**, *120*, 9387.
(57) Kim, Y. S.; Hochstrasser, R. M. *Proceedings of the National Academy of Sciences of the United States of America* **2005**, *102*, 11185.
(58) Chieffo, L.; Amsden, J.; Shattuck, J.; Hong, M. K.; Ziegler, L.; Erramilli, S. *Biophysical Review Letters* **2006**, *1*, 309.
(59) ; 2018 ed.; National Institute of Standards and Technology: Gaithersburg MD.
(60) Helbing, J.; Hamm, P. *J. Opt. Soc. Am. B* **2011**, *28*, 171.
(61) Dong, A.; Huang, P.; Zhao, X. J.; Sampath, V.; Caughey, W. S. *Journal of Biological Chemistry* **1994**, *269*, 23911.
(62) Shattuck, J. T.; Schneck, J. R.; Chieffo, L. R.; Erramilli, S.; Ziegler, L. D. *The Journal of Physical Chemistry B* **2013**, *117*, 15774.
(63) Shattuck, J.; Shah, P.; Erramilli, S.; Ziegler, L. D. *The Journal of Physical Chemistry B* **2016**, *120*, 10569.
(64) Chieffo, L. R.; Shattuck, J. T.; Pinnick, E.; Amsden, J. J.; Hong, M. K.; Wang, F.; Erramilli, S.; Ziegler, L. D. *The Journal of Physical Chemistry B* **2008**, *112*, 12776.
(65) Gorga, J. C.; Hazzard, J. H.; Caughey, W. S. *Archives of Biochemistry and Biophysics* **1985**, *240*, 734.
(66) Kubo, R. In *Advances in Chemical Physics*; John Wiley & Sons, Inc.: 2007, p 101.
(67) Kwak, K.; Park, S.; Finkelstein, I. J.; Fayer, M. D. *The Journal of Chemical Physics* **2007**, *127*, 124503.
(68) Kwac, K.; Cho, M. *The Journal of Physical Chemistry A* **2003**, *107*, 5903.
(69) Howdle, S. M.; Bagratashvili, V. N. *Chemical Physics Letters* **1993**, *214*, 215.
(70) Aubuchon, C. M.; Rector, K. D.; Holmes, W.; Fayer, M. D. *Chemical Physics Letters* **1999**, *299*, 84.
(71) Cottrell, T. L.; McCoubrey, J. C. *Molecular Energy Transfer in Gases*; Butterworths: London, 1961.
(72) Yardley, J. T.; Moore, C. B. *The Journal of Chemical Physics* **1968**, *49*, 1111.
(73) Flynn, G. W.; Parmenter, C. S.; Wodtke, A. M. *The Journal of Physical Chemistry* **1996**, *100*, 12817.
(74) Kenkre, V. M.; Tokmakoff, A.; Fayer, M. D. *The Journal of Chemical Physics* **1994**, *101*, 10618.
(75) Polanyi, J. C.; Woodall, K. B. *The Journal of Chemical Physics* **1972**, *56*, 1563.
(76) Gordon, R. G.; Klemperer, W.; Steinfeld, J. I. *Annual Review of Physical Chemistry* **1968**, *19*, 215.
(77) Holmes, R.; Jones, G. R.; Lawrence, R. *The Journal of Chemical Physics* **1964**, *41*, 2955.
(78) Jacobs, R. R.; Pettipiece, K. J.; Thomas, S. J. *Applied Physics Letters* **1974**, *24*, 375.
(79) Hinchen, J. J.; Hobbs, R. H. *The Journal of Chemical Physics* **1976**, *65*, 2732.
(80) Nicolaisen, H.-W.; Mäder, H. *Molecular Physics* **1991**, *73*, 349.

(81) Steinfeld, J. I.; Klemperer, W. *The Journal of Chemical Physics* **1965**, *42*, 3475.
(82) Park, C. *Journal of Thermophysics and Heat Transfer* **2004**, *18*, 527.
(83) Holmes, R.; Jones, G. R.; Lawrence, R. *Transactions of the Faraday Society* **1966**, *62*, 46.
(84) Holmes, R.; Jones, G. R.; Pusat, N. *Transactions of the Faraday Society* **1964**, *60*, 1220.

Table of Contents Entry:

Two-dimensional infrared spectroscopy from the gas to liquid phase:
Density dependent *J*-scrambling, vibrational relaxation, and the onset of liquid character

Greg Ng Pack[1,3], Matthew C. Rotondaro[1,3], Parth P. Shah[1,3], Aritra Mandal[4],

Shyamsunder Erramilli[2,3], and L.D. Ziegler[1,3*]

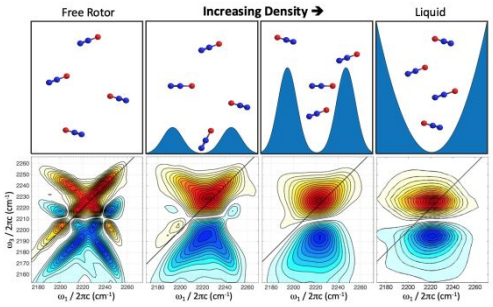

Ultrafast 2DIR reveals rotational relaxation rates, critical slowing effects, and co-existence of free rotor and liquid populations in supercritical fluids.